Anomalous thermodynamic properties in ferropericlase throughout its spin crossover transition

Z. Wu (吴忠庆),[1] J. F. Justo,[1,2] C. R. S. da Silva,[3] S. de Gironcoli,[4,5] and R. M. Wentzcovitch[1,3]
[1]*Department of Chemical Engineering and Materials Science, University of Minnesota, Minneapolis, Minnesota 55455, USA*
[2]*Escola Politécnica, Universidade de São Paulo, CP 61548, CEP 05424-970 São Paulo, SP, Brazil*
[3]*Minnesota Supercomputing Institute, University of Minnesota, Minneapolis, Minnesota 55455, USA*
[4]*Scuola Internazionale Superiore di Studi Avanzati, Trieste 34014, Italy*
[5]*DEMOCRITOS, National Simulation Center, Trieste 34014, Italy*
(Received 16 January 2009; revised manuscript received 4 May 2009; published 8 July 2009)

The thermodynamics properties of ferropericlase ($Mg_{1-x}Fe_xO$ where $x=0.1875$) (Fp) throughout its spin crossover were investigated by first principles. Fp was treated as an ideal solid solution of pure high-spin and low-spin states. The Gibbs free energies of the pure states were addressed using the LDA+U method. A vibrational virtual-crystal model was developed to address the vibrational properties of the pure spin cases and used in conjunction with quasiharmonic theory to compute their vibrational free energies. The thermodynamics properties of Fp display significant anomalies that should be typical of spin crossover systems in general. In Fp, in particular, they are fundamental for understanding the state of earth's interior, where the pressure and temperature conditions of the crossover are realized.

DOI: 10.1103/PhysRevB.80.014409 PACS number(s): 91.60.Pn, 75.30.Kz, 81.40.Rs

I. INTRODUCTION

Predictive first-principles calculations of thermodynamics properties of strongly correlated solid solutions are very challenging. In the case of spin crossover systems, this has not been attempted so far. The spin crossover phenomenon has been extensively studied during the last decades.[1] Very recently, pressure-induced spin crossovers in ferropericlase[2] (Fp), $Mg_{1-x}Fe_xO$, and ferrosilicate perovskite[3] (Pv), $Mg_{1-y}Fe_ySiO_3$, the major phases of the earth's lower mantle, have been identified. These discoveries have stimulated a large number of theoretical and experimental investigations[4–14] in a brief span of time. Spin crossovers can affect several materials' properties such as equations-of-state, elasticity, optical, and transport properties, all of which are fundamental for understanding the state of earth's interior. For example, the bulk modulus of Fp shows a dramatic softening during the crossover.[9,12] This should affect the interpretation of seismic data. Its absorption spectrum also shows considerable changes and this should affect radiative heat transport in the mantle. Therefore, understanding the thermodynamics properties of these materials at lower mantle conditions is important to build more realistic Earth's models.[15]

Fp is a solid solution of rocksalt-type MgO and FeO ($Mg_{1-x}Fe_xO$) with FeO being a minor component ($x\sim 0.18$ in the mantle). At low pressures, iron is in the high spin (HS) state, with $S=2$ (five d electrons up and one down). Under pressure, the electronic state of iron changes to the low spin (LS) with $S=0$ (three d electrons up and three down). There are several ways to rationalize this transition; it is essentially an enthalpy driven transition with a large volume collapse. It is also a crystal-field-induced transition. Under pressure, the crystal-field gap ($\Delta=E_{t2g}-E_{eg}$) increases and the internal energy is reduced (at constant volume) by doubly occupying the lower t_{2g} states, despite the penalty paid for the increase in the Coulomb correlation energy. Temperature affects this transition in a most remarkable way. It is a crossover, with the population of low spins, n, increasing continuously in a specific way.[8] The system passes through a mixed spin (MS) state upon application of pressure before it reaches the LS state. Earlier experimental data suggested an abrupt transition[5] but more recent investigations[9,10,13] have confirmed its continuous nature.

Here we predict the thermodynamics properties of Fp at relevant mantle conditions by combining first-principles calculations, the ideal solid solution (ISS) formalism, and quasiharmonic theory. We build on a previous calculation[8] of the static total energy of this material using the LDA+U method, with volume and spin-dependent U. However, now we develop a vibrational virtual-crystal model (VVCM) to compute the vibrational density of states (VDOS) of pure LS and HS states. These are strongly correlated solid solutions that play the role of end members in MS state of Fp. The free energy of Fp must include the vibrational contribution in investigations of thermodynamics properties. We now elaborate the ISS formalism and include vibrations to address the thermodynamics of the spin crossover.

This paper is organized as follows: in Sec. II we present the thermodynamics of the crossover in Fp, we describe the details of the static LDA+U total-energy calculation,[8] and describe the vibrational virtual-crystal model developed to compute VDOSs in solid solutions. The VDOSs are used in conjunction with the quasiharmonic approximation (QHA) to compute the free energy of the pure spin states. Finally we address the limit of validity of the QHA. Anomalous thermodynamics properties, such as thermal expansivity, thermal Grüneisen parameter, heat capacity, and bulk modulus, are reported in Sec. III. A summary is presented in Sec. IV.

II. METHODOLOGY

A. Thermodynamics of the mixed spin state

We describe Fp in the MS state as an ISS of pure HS and LS states. The Gibbs free energy of this MS state, $G(n,P,T)$, is then given by

$$G(n,P,T) = nG_{\mathrm{LS}}(P,T) + (1-n)G_{\mathrm{HS}}(P,T) + G_{mix}, \quad (1)$$

where $n=n(P,T)$ is the fraction of LS states, G_{LS} and G_{HS} are, respectively, the Gibbs free energies of the pure LS and HS states and G_{mix} is the free energy of mixing of the ideal HS/LS mixture. Although we adopt the ISS formalism, the calculation reported here accounts for all interactions in the solid solution, including interactions between irons, for the particular atomic configuration we adopted. The assumption of an ISS, i.e., noninteracting solution, is very robust up to the iron concentrations investigated here, $X_{\mathrm{Fe}}=0.1875$, since up to this concentration the first-principles crossover pressure is independent of iron concentration X_{Fe} as well as of the low-spin fraction set from the start.[8] The regular solution approximation was used by Slichter and Drickamer[16] in the past to develop a similar model. Their model introduces the effects of both the difference in compressibility of the HS and LS states and pressure dependence of compressibility of HS and LS states. In the present work, these effects are described by first principles without the need to introduce any parameters. Slichter and Drickamer discussed both ideal solution and regular solution in their model. However, in the present work, we only considered the ideal solution. Several facts derived from static calculations suggest that the ISS treatment is appropriate. These include the facts that the crossover pressure is independent of iron concentration, up to the concentration reported here, and that the volume of the mixed-spin state is linearly dependent on the low-spin fraction. Notice that we do not assume Fp to be an ISS of MgO and FeO. We assume that MS Fp is an ISS of LS Fp and HS Fp. It is the Fe-Fe interaction that is considered negligible in our calculations. Improvement in the treatment of the solid solution by considering the effect of other atomic configurations is desirable, but it is beyond what we can afford calculating today. It is well known that larger iron concentrations increase the onset of the crossover pressure[13] clearly indicating inter-iron interactions. This broadens the crossover pressure range. Our calculations, as are, cannot account for this effect. By considering an ensemble of atomic configurations, each with its own onset pressure and its own parameter U computed by first principles, the most challenging part of the calculation, one could reproduce the finite width of the crossover even at 0 K. When the interaction becomes very strong, presumably at high iron concentration, the crossover should turn into a transition. Nevertheless, we believe that this treatment of the spin crossover in Fp describes the phenomenon very well, particularly at high temperatures.

The molar Gibbs free energy of the pure (HS/LS) states is

$$G_{\mathrm{HS/LS}}(P,T) = G^{stat+vib}_{\mathrm{HS/LS}}(P,T) + G^{mag}_{\mathrm{HS/LS}}, \quad (2)$$

where $G^{stat+vib}_{\mathrm{HS/LS}}(P,T)$ is the Gibbs free energy containing static and vibrational contributions and $G^{mag}_{\mathrm{HS/LS}}$ is the magnetic contribution,

$$G^{mag}_{\mathrm{LS}} = 0 \quad (3a)$$

$$G^{mag}_{\mathrm{HS}} = -k_B T X_{\mathrm{Fe}} \ln[m(2S+1)] \quad (3b)$$

where $S=2$ and $m=3$ are, respectively, the spin and electronic configuration (orbital) degeneracies of iron in HS state. This is a purely entropic contribution to the free energy.

The free energy of mixing is given by

$$G_{mix}(n) = -TS_{mix}(n) = k_B T X_{\mathrm{Fe}}[n \ln n + (1-n)\ln(1-n)], \quad (4)$$

where the entropy of mixing is assumed to be that of an ISS. This is a well justified approximation in the present case.[7] Minimization of the free energy in Eq. (1) with respect to the LS fraction, n, leads to

$$n(P,T) = \frac{1}{1 + m(2S+1)\exp\left[\dfrac{\Delta G^{stat+vib}_{\mathrm{LS-HS}}}{X_{\mathrm{Fe}} K_B T}\right]}, \quad (5)$$

where $\Delta G^{stat+vib}_{\mathrm{LS-HS}} = G^{stat+vib}_{\mathrm{LS}} - G^{stat+vib}_{\mathrm{HS}}$. This expression of $n(P,T)$ differs from a previous derivation[8] by the presence of $\Delta G^{stat+vib}_{\mathrm{LS-HS}}$ in the exponent, as opposed to $\Delta H_{\mathrm{LS-HS}}$. Here we have included the vibrational contribution to the free energy, which is spin dependent. As it will be shown in Sec. III, the inclusion of the vibrational energy shifts the spin crossover pressure range to higher pressures, improving considerably the agreement with experimental results[1,5,9] compared to previous results[8] (to be shown below). From the Gibbs free energy of Eq. (1), all the thermodynamics properties can be obtained by using standard thermodynamics relations. We illustrate the origin of the anomalies in the thermodynamics properties by inspecting the thermal expansivity as an example.

The volume of the MS state is

$$V(n) = \left.\frac{\partial G(n)}{\partial P}\right|_T = \left.\frac{\partial G(n)}{\partial P}\right|_{T,n} + \left.\frac{\partial G(n)}{\partial n}\right|_{T,P} \left.\frac{\partial n}{\partial P}\right|_T. \quad (6)$$

Since at equilibrium $\partial G(n)/\partial n|_{T,P}=0$, one gets

$$V(n) = nV_{\mathrm{LS}}(P,T) + (1-n)V_{\mathrm{HS}}(P,T), \quad (7)$$

where $V_{\mathrm{HS/LS}}(P,T) = \frac{\partial G_{\mathrm{HS/LS}}}{\partial P}|_T$ are the volumes of the pure HS/LS states. As expected, this is the volume of an ISS. This relationship $(0 \le n(P,T) \le 1)$ was shown to be very accurate in static calculations.[8] A similar linear relationship is now derived at high temperatures by assuming an ISS. The thermal-expansion coefficient of the MS state, $\alpha(n) = \frac{1}{V(n)}\left(\frac{\partial V(n)}{\partial T}\right)_P$ [short for $\alpha(n,P,T)$] is then

$$\alpha(n)V(n) = nV_{\mathrm{LS}}\alpha_{\mathrm{LS}} + (1-n)V_{\mathrm{HS}}\alpha_{\mathrm{HS}} + (V_{\mathrm{LS}} - V_{\mathrm{HS}}) \left.\frac{\partial n}{\partial T}\right|_P, \quad (8)$$

where $\alpha_{\mathrm{HS/LS}}$ are the respective expansivities of pure HS/LS states. The last term in Eq. (8) is the source of the anomaly caused by the crossover, within which $\frac{\partial n}{\partial T}|_P \neq 0$. Similarly, the isothermal bulk modulus of the MS state, $K^T(n)$, is given by

$$\frac{V(n)}{K^T(n)} = n\frac{V_{\mathrm{LS}}}{K^T_{\mathrm{LS}}} + (1-n)\frac{V_{\mathrm{HS}}}{K^T_{\mathrm{HS}}} - (V_{\mathrm{LS}} - V_{\mathrm{HS}}) \left.\frac{\partial n}{\partial P}\right|_T \quad (9)$$

where $K^T_{\mathrm{HS/LS}}$ are the isothermal bulk moduli of pure HS/LS states. Notice again the presence of a third term proportional to $\frac{\partial n}{\partial P}|_T$ in Eq. (9), which is nonvanishing during the crossover. These nonvanishing derivatives of n with respect to T or P impact all thermodynamics properties. This is easily observed for properties such as the adiabatic bulk modulus and thermal Grüneisen parameter

$$K^S = K^T\left[1 + \frac{\alpha^2 K^T V}{C_V}\right], \quad (10)$$

$$\gamma_{\mathrm{th}} = \frac{\alpha K_T V}{C_V}. \quad (11)$$

Equation (1) shows that the starting point of this calculation are the free energies, of pure HS/LS states, $G_{\mathrm{LS/LS}}(P,T)$, at the desired conditions. These also give $n(P,T)$ [Eq. (5)]. Here, these free energies were obtained by combining first-principles static total-energy calculations[7] with quasiharmonic calculations of the vibrational free energy.

B. Static properties of the pure spin states

The static properties of the pure HS/LS states were computed by first principles. The calculations are very similar to those reported in Ref. 8. The electronic wave functions were expanded in a plane-wave basis set with a cutoff of 70 Ry. The Brillouin zone of the 64-atoms supercell was sampled by a $2\times2\times2$ Monkhorst-Pack grid of k points. The calculations were performed using a rotationally invariant version of the LDA+U method, where U was computed by an internally consistent procedure.[17] The values of U used here are the same as those used in Ref. 8, which are spin and volume dependent. Atomic positions were fully relaxed in all calculations. The oxygen pseudopotential was generated using the Troullier-Martins method,[18] in a $2s^2 2p^4$ configuration with local p orbital. The magnesium pseudopotential was generated using the von Barth-Car method,[19] with five electronic configurations ($3s^2 3p^0$, $3s^1 3p^1$, $3s^1 3p^{0.5} 3d^{0.5}$, $3s^1 3p^{0.5}$, and $3s^1 3d^1$, respectively, with weights of 1.5, 0.6, 0.3, 0.3, and 0.2) with d-channel locality. The iron pseudopotential was generated using the modified Rappe-Rabe-Kaxiras-Joannopoulos method[20] in a $3d^7 4s^1$ configuration.

The 64-atoms supercell contained 26 magnesium, 32 oxygen, and 6 iron atoms, corresponding to $X_{\mathrm{Fe}}=0.1875$. Ferrous irons were placed on magnesium sites in a reference rocksalt structure. Irons were placed in sites that maximized the inter-iron distances within the supercell. This iron concentration appears to be the upper concentration limit for which iron-iron interactions can be neglected in the thermodynamics formalism.

C. The vibrational virtual-crystal model

The calculation discussed in the previous section allowed us to obtain the static properties of Fp in the pure LS and HS states. The Helmholtz free energies of these states were computed within the QHA[21]

$$F(V,T) = \left[U(V) + \sum_{qj}\frac{\hbar\omega_{qj}(V)}{2}\right] + k_B T\sum_{qj}\ln\left[1 - \exp\left(-\frac{\hbar\omega_{qj}(V)}{k_B T}\right)\right], \quad (12)$$

where $U(V)$ and $\omega(V)$ are the volume-dependent static internal energy and the phonon spectrum, respectively. Since Fp is a 2.6–3.0 eV insulator,[8] the thermal energy from electronic excitations can be neglected. Current methodological limitations preclude the direct computation of the VDOS within the LDA+U approach, especially in a solid solution. To circumvent this problem, we developed a VVCM within the same spirit of the vibrational model described in Ref. 22. The VVCM entails replacing the atomic species forming the solid solution, in this case magnesium and HS or LS irons, by an "average" cation that reproduces the same vibrational properties of the solid solution. This virtual-crystal approximation has been popular in electronic structure theory[22–24] but here we use this concept with the purpose of computing vibrational and thermodynamics properties only. The development of successful VVCMs would be extremely useful for computations of VDOSs of solid solutions, especially those involving strongly correlated ions so common in minerals.

The VVCMs for pure HS/LS states consist of two atoms per cell in the rocksalt structure; oxygen and a virtual cation with mass

$$M^{cation}_{\mathrm{VC}} = (1 - X_{\mathrm{Fe}})M_{\mathrm{Mg}} + X_{\mathrm{Fe}}M_{\mathrm{Fe}}, \quad (13)$$

where M_{Mg} and M_{Fe} are, respectively, the atomic masses of magnesium and iron, the latter being spin independent. These VVCMs are essentially periclase (MgO) with modified cation masses and modified interatomic-force constants that reproduce the static elastic constants of Fp in pure spin states. The force constants of periclase were first computed using density-functional perturbation theory.[25] The force constants of the HS/LS VCs were then obtained by matching the elastic constants ($C_{\sigma\tau\alpha\beta}$) extracted from their acoustic phonon dispersion near $k=0$ to the elastic constants obtained directly by first principles, i.e., from the stress versus strain relation. There is a linear relationship between force constants, $D_{\mu\nu}(R^{ij}) = D^{ij}_{\mu\nu}$, and elastic constants, $C_{\sigma\tau\alpha\beta}$,[26]

$$C_{\sigma\tau\alpha\beta}(V) = \sum_{(i,j),(\mu,\nu)} a^{ij}_{\mu\nu,\sigma\tau\alpha\beta}(V) D^{ij}_{\mu\nu}(V). \quad (14)$$

Greek letters in Eq. (14) refer to Cartesian indices and i,j refer to atom indices. $C_{\sigma\tau\alpha\beta}(V)$ are the volume-dependent elastic constants in Cartesian notation, while $D^{ij}_{\mu\nu}$ are the interatomic-force constants for displacements in directions μ and ν between atoms i and j separated by $\boldsymbol{R}^{ij}$. The summation in Eq. (14) is over all atomic pairs (i,j) and $a^{ij}_{\mu\nu,\sigma\tau\alpha\beta}(V)$ represent a set of volume-dependent constants. Due to symmetry constrains, several $a^{ij}_{\mu\nu,\sigma\tau\alpha\beta}$ vanish. Additionally, Eq. (14) is a convergent summation, since the force constants vanish rapidly with the interatomic distances. The convergence is guaranteed if the force constants vanish faster than

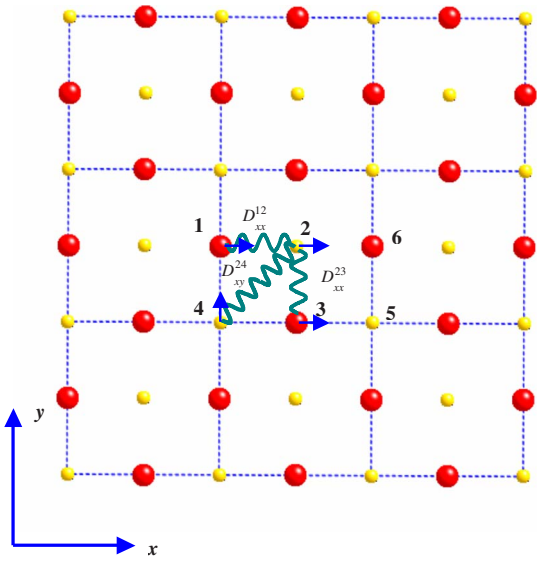

FIG. 1. (Color online) Schematic representation of the three largest force constants of periclase in xy plane: the Mg-O nearest-neighbor longitudinal interaction $D_{xx}^{12}(V)$, the Mg-O nearest-neighbor transverse interaction $D_{xx}^{23}(V)$, and the Mg-Mg nearest-neighbor interaction $D_{xy}^{24}(V)$. Oxygen and magnesium are represented by large (red) and small (yellow) spheres, respectively.

$1/R^5$, where R is the interatomic separation,[26] which is the case here. There are essentially three relevant force constants in Fp, which were obtained by modifying the corresponding force constants of periclase taking into account Eq. (14).

The force constants of periclase, defined as

$$D_{\mu\nu}^{ij} = \frac{\partial^2 E(R^{ij})}{\partial R_i^\mu \, \partial R_j^\nu}, \tag{15}$$

were computed using density-functional perturbation theory.[25] Phonon dispersions are then obtained at each volume

$$\det \left| \frac{D_{\mu\nu}^{ij}(V)}{\sqrt{M_i M_j}} - \omega^2 \right| = 0. \tag{16}$$

Longitudinal and transverse phonon velocities along any propagation direction, $[\vec{n}]$, are then obtained from

$$V_{L/T}[\vec{n}] = \frac{d\omega_{LA/TA}}{dq}[\vec{n}]\bigg|_{q=0} \tag{17}$$

These velocities can also be obtained by computing the single-crystal elastic constants ($C_{\sigma\tau\alpha\beta}$) and then solving Cristoffel's equation[27]

$$\det|C_{\sigma\tau\alpha\beta} n_\tau n_\beta - \rho V^2 \delta_{\sigma\alpha}| = 0, \tag{18}$$

where $[\vec{n}]$, ρ, V, and $\delta_{\sigma\alpha}$ are, respectively, the propagation direction, density, wave velocity, and Kroenecker delta. Both Fp and periclase[28] are cubic systems and have only three elastic constants, C_{11}, C_{12}, and C_{44} (in Voigt notation). The longitudinal (V_L) and transverse (V_T) wave velocities along [100] are

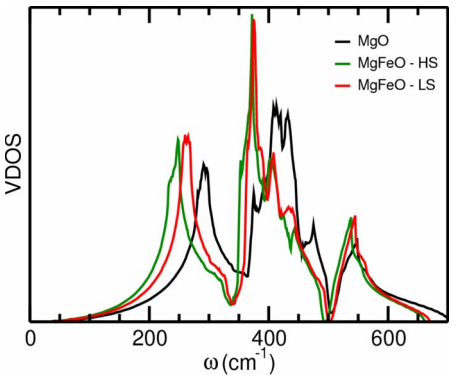

FIG. 2. (Color online) Vibrational density of states of MgO (black) and Fp in the HS (green) and LS (red) states. These VDOS were computed with a lattice parameter a=4.21 Å.

$$V_L = \omega_L/q = \sqrt{C_{11}/\rho},$$

$$V_T = \omega_T/q = \sqrt{C_{44}/\rho}, \tag{19}$$

and along [110] are

$$V_L = \sqrt{(C_{11} + C_{12} + 2C_{44})/2\rho},$$

$$V_{T1} = \sqrt{C_{44}/\rho},$$

$$V_{T2} = \sqrt{(C_{11} - C_{12})/2\rho}. \tag{20}$$

The point now is to obtain $D_{\mu\nu}^{ij}(V)$ for the VVCMs in pure HS or LS states. We modify the force constants [Eq. (15)] of periclase such that the acoustic phonon velocities [Eq. (17)] produced matched those obtained from the solution of Cryst-offel's equation [Eq. (18)] along particular directions [Eqs.

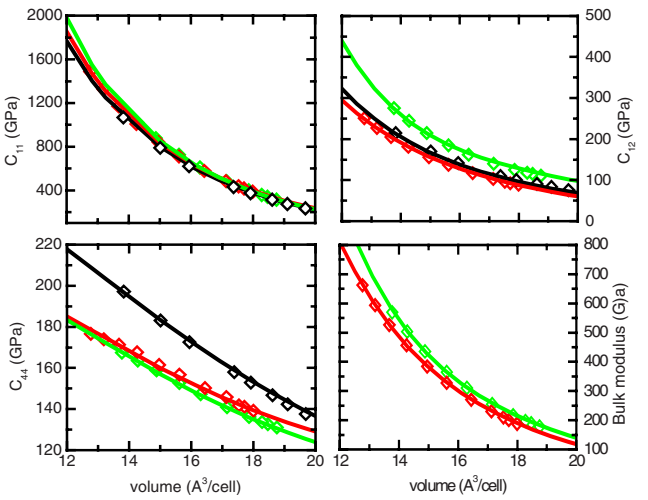

FIG. 3. (Color online) Elastic constants obtained by first principles from the stress versus strain relation (symbols) and from phonon velocities (lines) [see Eqs. (15)–(20)]. The acoustic phonon velocities MgO (black) are computed directly using density-functional perturbation theory. The phonon velocities of Fp in HS (green) and LS (red) were obtained by modifying the force constants of MgO (see text and Table I).

TABLE I. The eight largest force constants of periclase (MgO) and their modified values for Fp in HS and LS states. These values are obtained for a lattice constant equal to 4.07 Å.

	D_{xx}^{12}	D_{xy}^{24}	D_{xx}^{23}	D_{xx}^{13}	D_{xx}^{45}	D_{xx}^{24}	D_{xx}^{16}	D_{zz}^{13}
MgO	−0.15165	−0.015259	0.01172	−0.00775	−0.00536	−0.00472	0.00455	−0.00338
HS	−0.15703	−0.016991	0.01726	−0.00775	−0.00536	−0.00472	0.00455	−0.00338
LS	−0.15714	−0.011784	0.01624	−0.00775	−0.00536	−0.00472	0.00455	−0.00338

(19) and (20)]. The elastic constants used in Eq. (18) were computed by first principles separately for HS and LS Fp. Figure 1 indicates the three largest and most relevant force constants of periclase in xy plane. These are: (a) the Mg-O nearest-neighbor longitudinal constant, $D_{xx}^{12}(V)$, (b) the Mg-O nearest-neighbor transverse constant, $D_{xx}^{23}(V)$, and (c) the Mg-Mg nearest-neighbor magnesium interaction constant, $D_{xy}^{24}(V)$. Their values are given in Table I. All the other force constants have minor effects in the acoustic dispersions. D_{xx}^{13}, D_{xx}^{16}, and D_{zz}^{13} are force constants between O atoms and the replacement of Mg by Fe in the VC affect these force constants in Fp very little. D_{xx}^{45} and D_{xx}^{24} are force constants between Mg and O but they are quite smaller than the three major constants. The other force constants are even smaller than those constants presented in the Table I indicating the rapid convergence of summation in Eq. (14). Therefore, only the three largest force constants of periclase were modified to describe Fp in pure spin states.

The VDOS of periclase, HS, and LS VVCMs are shown in Fig. 2. Figure 3 shows that the elastic constants and bulk modulus of HS and LS states computed from the phonon velocities agree well with those computed directly from the stress versus strain relations in LDA+U calculations. Therefore the VVCMs' acoustic phonon dispersions are precisely the same as those of HS and LS Fp. This ensures that the thermodynamics properties are calculated using the correct VDOS at low frequencies and with a reasonably good, i.e., representative, VDOS at high frequencies. The VVCM in conjunction with the QHA should provide more suitable vibrational and thermodynamics properties than a Mie-Debye-Grüneisen model.

D. Range of validity of the QHA

The pressure/temperature range of validity of the QHA was carefully considered. Its upper temperature limit of validity at a certain pressure can be indicated by the inflection point in the thermal expansivity versus temperature curve,[29,30] i.e., $\partial^2\alpha/\partial T^2|_P=0$. Beyond this inflection point, the thermal expansivity deviates from the usually linear behavior of experimental measurements.[30] We first established this temperature limit for Fp in the HS and LS states. The expansivity of the MS state is related to those of the LS and HS states through Eq. (8). The maximum temperature limit for our predictions in the MS state was chosen as the minimum of those limits established for the HS and LS states. Dashed lines in Figs. 4 and 7 indicate temperatures above this limit.

III. RESULTS AND DISCUSSION

All the approximations described in the previous section provided an excellent description of Fp in the MS state at finite temperatures and pressures. This is confirmed in Fig. 4, in which the isothermal compression curves of Fp ($X_{\mathrm{Fe}}=0.1875$) are compared to available experimental data.[5,13] At 300 K, the isotherm displays an anomaly in $V(P,T,n)$ that is consistent with the experimental results. The theoretical equilibrium volume at 300 K, 11.46 $\mathrm{cm}^3/\mathrm{mol}$, is slightly larger than the experimental one,[5] 11.35 $\mathrm{cm}^3/\mathrm{mol}$. This difference is consistent with the small difference between experimental and calculated iron concentrations. The theoretical volume reduction due to the iron spin collapse is in average 4.2% throughout the pressure range of the crossover, compared to about 3–4 % from experiments.[5] At higher temperatures, the anomalies are smaller and their pressure ranges larger.

Figure 5 shows the LS fraction in Fp, as computed by Eq. (5), as a color map. At 0 K, the transition is very sharp and occurs at ~36 GPa. With increasing temperature, the transition pressure increases and the transition broadens. This figure also shows the changes in the transition pressures after inclusion of the vibrational effects. Even at 0 K, there is an increase of 2.5 GPa in the transition pressure due to zero-point motion. At $T=300$ K, the center of the transition, i.e., for $n(P,T)=0.5$, occurs at 39.5 GPa, which should be com-

TABLE II. Thermodynamics properties of periclase and Fp (in pure HS state) at ambient conditions, as compared to experimental data (Refs. 36–38). The table presents the volume, thermal-expansion coefficient, Grüneisen parameter, heat capacity, and adiabatic bulk modulus.

	V (A^3/cell)	α (10^{-5}/K)	γ_{th}	C_P (J mol^{-1} K^{-1})	C_V (J mol^{-1} K^{-1})	K_S (GPa)	
$Mg_{0.8125}Fe_{0.1875}O$	19.04	3.35	1.73	39.66	38.98	172.48	Calculation
MgO	18.80	3.16	1.55	37.64	37.09	163.07	
MgO	18.69	3.12	1.54	37.67		163.2	Experiment

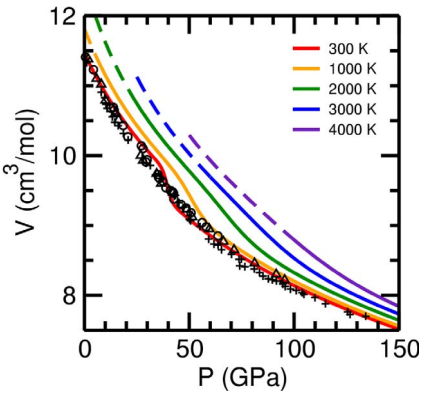

FIG. 4. (Color online) Compression curves of $Mg_{1-x}Fe_xO$ ($x=0.1875$) along several isotherms. Full (dashed) lines correspond to results within (outside) the *PT* regime of validity of the QHA. Plus symbols are experimental results for $X_{exp}=0.17$ presented in Ref. 5 and circle and triangle symbols are experimental results for $X_{exp}=0.2$ presented in Ref. 13.

pared to the experimental transition pressures at room temperature around 50–55 GPa.[5,13] Fig. 6 shows the pressure dependence of the LS fraction at several temperatures and the respective derivatives $\partial n/\partial P|_T$. Figure 6(a) shows that vibrational effects become more significant with increasing temperature, shifting the crossover pressure range to higher pressures.

The rapid change in the LS fraction during the crossover leads to dramatic effects on the thermodynamics properties of Fp. The origin of these anomalies is the dependence of these properties on $\partial n/\partial T|_P$ [see Fig. 6(b)]. Figure 7 shows the thermal expansivity, constant-pressure heat capacity, thermal Grüneisen parameter, and adiabatic bulk modulus of Fp in the MS state. At very low (under 30 GPa) or very high (over 100 GPa) pressures, these properties appear to have a normal behavior, since the system remains in HS and LS states, respectively. The thermal expansivity at 0 GPa (see Table II), i.e., in the HS state, is essentially the same as that of MgO.[28] This result is consistent with experimental observations that this coefficient is independent of the iron concentration.[31] At 100 GPa and above ~1500 K HS Fp

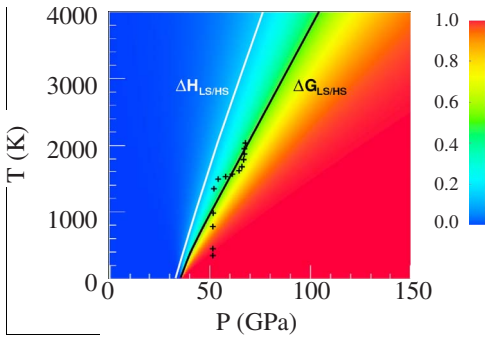

FIG. 5. (Color online) "Phase diagram" of Fp with $x=0.1875$. The black and white lines correspond to the middle point of the crossover, where $n(P,T)=0.5$, computed with and without including the vibrational contribution to the free energy, respectively. The plus symbols are experimental data corresponding to $n=0.5$ (Ref. 9).

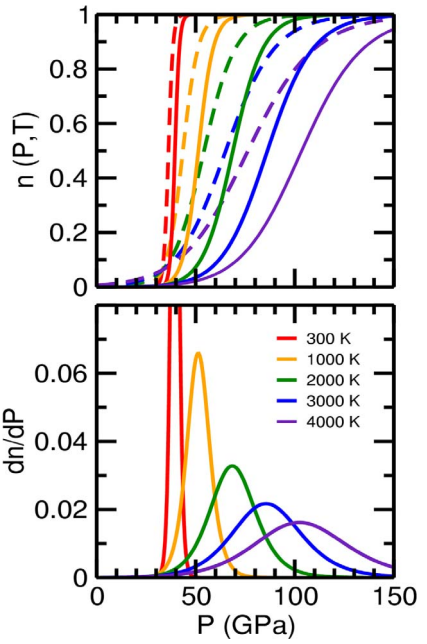

FIG. 6. (Color online) (a) LS fraction, $n(P,T)$, of Fp with $x=0.1875$ as a function of pressure along several isotherms. The figure presents the results with (full lines) and without (dashed lines) including the vibrational contribution to free energies. (b) Derivatives $\partial n/\partial P$ at the same temperatures as (a).

starts reentering the MS state and the anomaly starts showing again. The thermal expansivity increases substantially throughout the spin crossover. It is almost five times larger at the peak of the anomaly. The anomaly in thermal Grüneisen

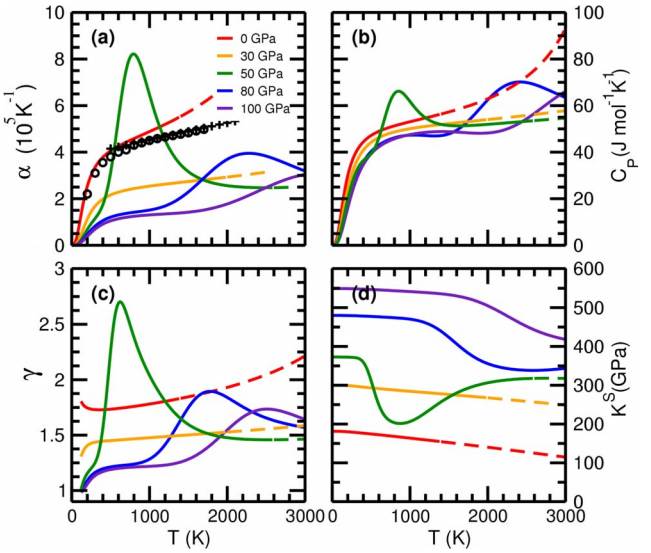

FIG. 7. (Color online) Thermodynamics properties of Fp as a function of temperature along several isobars. The figure presents (a) thermal-expansion coefficient, (b) heat capacity at constant pressure, (c) thermal Grüneisen parameter, and (d) adiabatic bulk modulus. Full (dashed) lines correspond to results within (outside) the *PT* regime of validity of the QHA. Circles and crosses in (a) are experimental thermal expansivities at 0 GPa for $Mg_{1-x}Fe_xO$, respectively, with $x=0.0$ (Ref. 38) and with $x=0.36$ (Ref. 31).

TABLE III. Temperature in K at the extreme values of the anomaly for various thermodynamics properties.

	$(\partial n/\partial T)_P$	α	γ_{th}	C_P	K_S
40 GPa	300	300	180	360	320
60 GPa	1300	1300	1020	1370	1400

parameter is the next most affected, being almost twice larger at the peak. The anomaly in the heat capacity is not as dramatic as in the thermal expansivity and Grüneisen parameter. The bulk modulus, an important quantity for interpretation of seismic data, shows considerable softening throughout the crossover. Fp is likely to consist approximately 20 vol % of the lower mantle. The PT range of this region is $23<P<135$ GPa and $2000<T<4000$ K. As shown in this paper, the spin crossover in Fp falls precisely in the middle of this range. Therefore, all these anomalous properties are fundamental new ingredients in modeling the lower mantle and are likely to profoundly affect our understanding of this region.

As listed in Table III, the temperatures corresponding to the extreme values of the thermodynamics properties differ. The temperature at the extreme value of the thermal expansion is the same to the one of the temperature derivative of LS fraction since the term causing this anomaly is proportional to $\partial n/\partial T|_P$ [see Eq. (8)]. This implies that the critical crossover temperature derived from magnetic and lattice measurements should be similar, which was really observed in the spin crossover of iron(II) tris(2-(2′-pyridyl)benzimidazole) complex.[32] The temperature at the peak of the specific heat, however, is shifted to higher temperatures because of its linear dependence on T: $C_P=T(\partial S/\partial T)_P$. Temperature usually decreases the bulk modulus linearly and shifts the temperature at the minimum to higher temperature. The thermal Grüneisen parameter is $\gamma_{\text{th}}=\alpha K_S V/C_P$. The softening of K_S and rapid increase in C_P in the crossover region shift the peak temperature of γ_{th} to lower temperatures. The difference between the extreme-value temperatures in heat capacity and in the Grüneisen parameter increases from 180 K at 40 GPa to 350 K at 60 GPa with a simultaneous broadening of the crossover region.

IV. SUMMARY

In summary, we have investigated the role of the spin crossover on the thermodynamics properties of Fp. The material was described as an ISS of HS and LS Fp. We developed a vibrational virtual-crystal model to compute the vibrational density of states of the pure spin components. The thermodynamics method presented here is quite general and applicable to spin crossover systems with small spin concentrations.

We showed that the vibrational contribution to the free energy plays an important role in the HS to LS transition, consistent with what has been found in several magnetic materials.[33–35] Inclusion of the vibrational free energy shifts the transition pressure range of Fp to higher pressures, improving agreement with experiments.[5–7] The spin crossover causes anomalies on the thermodynamics properties of Fp, such as large increase in the thermal-expansion coefficient and thermal Grüneisen parameter, a noticeable change in specific heat, and a substantial softening of the bulk modulus. The latter has recently been observed experimentally.[10]

ACKNOWLEDGMENTS

This research was supported by NSFunder Grants No. EAR 0635990 and No. DMR 0325218 (ITAMIT) through the University of Texas and by NSF under Grant No. ATM 0428774 (VLAB). J.F.J. acknowledges partial support by the Brazilian agency CNPq. Calculations were performed with the Quantum ESPRESSO package.[39] Computer time was provided by the Minnesota Supercomputer Institute.

[1] *Topics in Current Chemistry*, Spin Crossover in Transition Metal Compounds I-III Vol. 233-235, edited by P. Gotlich and H. A. Goodwin (Springer, New York, 2004).
[2] J. Badro, G. Fiquet, F. Guyot, J. P. Rueff, V. V. Struzhkin, G. Vankó, and G. Monaco, Science **300**, 789 (2003).
[3] J. Badro, J. P. Rueff, G. Vankó, G. Monaco, G. Fiquet, and F. Guyot, Science **305**, 383 (2004).
[4] W. Sturhahn, J. M. Jackson, and J. F. Lin, Geophys. Res. Lett. **32**, L12307 (2005).
[5] J. F. Lin, V. V. Struzhkin, S. D. Jacobsen, M. Y. Hu, P. Chow, J. Kung, H. Z. Liu, H. K. Mao, and R. J. Hemley, Nature (London) **436**, 377 (2005).
[6] S. Speziale, A. Milner, V. E. Lee, S. M. Clark, M. P. Pasternak, and R. Jeanloz, Proc. Natl. Acad. Sci. U.S.A. **102**, 17918 (2005).
[7] A. F. Goncharov, V. V. Struzhkin, and S. D. Jacobsen, Science **312**, 1205 (2006).
[8] T. Tsuchiya, R. M. Wentzcovitch, C. R. S. da Silva, and S. de Gironcoli, Phys. Rev. Lett. **96**, 198501 (2006).
[9] J. F. Lin, G. Vankó, S. D. Jacobsen, V. Iota, V. V. Struzhkin, V. B. Prakapenka, A. Kuznetsov, and C. S. Yoo, Science **317**, 1740 (2007).
[10] J. C. Crowhurst, J. M. Brown, A. F. Goncharov, and S. D. Jacobsen, Science **319**, 451 (2008).
[11] A. Bengtson, K. Persson, and D. Morgan, Earth Planet. Sci. Lett. **265**, 535 (2008).

[12] R. M. Wentzcovitch, J. F. Justo, Z. Wu, C. R. S. da Silva, D. A. Yuen, and D. Kohlstedt, Proc. Natl. Acad. Sci. U.S.A. **106**, 8447 (2009).
[13] Y. Fei, Li Zhang, Alexandre Corgne, Heather Watson, Angele Ricolleau, Yue Meng, and Vitali Prakapenka, Geophys. Res. Lett. **34**, L17307 (2007).
[14] J. F. Lin and T. Tsuchiya, Phys. Earth Planet. Inter. **170**, 248 (2008).
[15] A. M. Dziewonski and D. L. Anderson, Phys. Earth Planet. Inter. **25**, 297 (1981).
[16] C. P. Slichter and H. G. Drickamer, J. Chem. Phys. **56**, 2142 (1972).
[17] M. Cococcioni and S. de Gironcoli, Phys. Rev. B **71**, 035105 (2005).
[18] N. Troullier and J. L. Martins, Phys. Rev. B **43**, 1993 (1991).
[19] For a brief description of the methods, see A. Dal Corso, S. Baroni, R. Resta, and S. de Gironcoli, Phys. Rev. B **47**, 3588 (1993).
[20] A. M. Rappe, K. M. Rabe, E. Kaxiras, and J. D. Joannopoulos, Phys. Rev. B **41**, 1227 (1990).
[21] D. Wallace, *Thermodynamics of Crystals* (Wiley, New York, 1972).
[22] S. de Gironcoli, P. Giannozzi, and S. Baroni, Phys. Rev. Lett. **66**, 2116 (1991).
[23] L. Bellaiche, S. H. Wei, and A. Zunger, Appl. Phys. Lett. **70**, 3558 (1997).
[24] D. A. Papaconstantopoulos and W. E. Pickett, Phys. Rev. B **57**, 12751 (1998).
[25] S. Baroni, S. de Gironcoli, A. Dal Corso, and P. Giannozzi, Rev. Mod. Phys. **73**, 515 (2001).
[26] N. W. Ashcroft and N. D. Mermin, *Solid State Physics* (Holt, Rinehart, and Winston, New York, 1976).
[27] M. J. P. Musgrave, *Crystal Acoustics* (Holden-Day, San Francisco, 1970).
[28] B. B. Karki, R. M. Wentzcovitch, S. de Gironcoli, and S. Baroni, Phys. Rev. B **61**, 8793 (2000).
[29] R. M. Wentzcovitch, B. B. Karki, M. Cococcioni, and S. de Gironcoli, Phys. Rev. Lett. **92**, 018501 (2004).
[30] P. Carrier, J. F. Justo, and R. M. Wentzcovitch, Phys. Rev. B **78**, 144302 (2008).
[31] W. van Westrenen, J. Li, Y. W. Fei, M. R. Frank, H. Hellwig, T. Komabayashi, K. Mibe, W. G. Minarik, J. A. van Orman, H. C. Watson, K. Funakoshi, and M. W. Schmidt, Phys. Earth Planet. Inter. **151**, 163 (2005).
[32] R. Boca, M. Boca, H. Ehrenberg, H. Fuess, W. Linert, F. Renz, and I. Svoboda, Chem. Phys. **293**, 375 (2003).
[33] D. M. Adams and D. N. Hendrickson, J. Am. Chem. Soc. **118**, 11515 (1996).
[34] M. Sorai and S. Seki, J. Phys. Chem. Solids **35**, 555 (1974).
[35] J. P. Tuchagues, A. Bousseksou, G. Molnar, J. J. McGarvey, and F. Varret, Top. Curr. Chem. **235**, 85 (2004).
[36] D. G. Isaak, O. L. Anderson, and T. Goto, Phys. Chem. Miner. **16**, 704 (1989).
[37] Y. Fei, Am. Mineral. **84**, 272 (1999).
[38] Y. S. Touloukian, R. K. Kirdby, R. E. Taylor, and T. Y. R. Lee, *Thermophysical Properties of Matter* (Plenum, New York, 1977), Vol. 13.
[39] P. Giannozzi *et al.*, arXiv:0906.2569.